

See discussions, stats, and author profiles for this publication at: <https://www.researchgate.net/publication/259477599>

Epitaxial Growth of Au@Ni Core–Shell Nanocrystals Prepared Using a Two-Step Reduction Method

ARTICLE in CRYSTAL GROWTH & DESIGN · MAY 2011

Impact Factor: 4.89 · DOI: 10.1021/cg200199b

CITATIONS

34

READS

33

4 AUTHORS, INCLUDING:



Masaharu Tsuji

Kyushu University

441 PUBLICATIONS 6,237 CITATIONS

[SEE PROFILE](#)

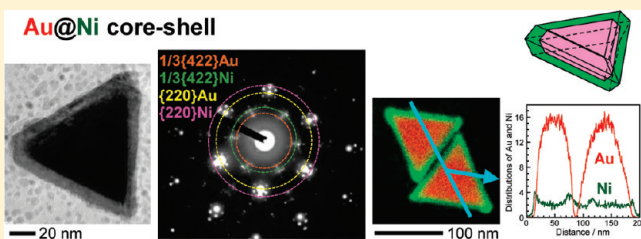
Epitaxial Growth of Au@Ni Core–Shell Nanocrystals Prepared Using a Two-Step Reduction Method

Masaharu Tsuji,^{*,†,‡} Daiki Yamaguchi,[‡] Mika Matsunaga,[†] and Koji Ikeda[‡]

[†]Institute for Materials Chemistry and Engineering and [‡]Department of Applied Science for Electronics and Materials, Graduate School of Engineering Sciences, Kyushu University, Kasuga 816-8580, Japan

 Supporting Information

ABSTRACT: Au@Ni core–shell nanocrystals were prepared using a two-step reduction method. First, mixtures of octahedral, triangular and hexagonal platelike, decahedral, and icosahedral Au core seeds were prepared by reducing $\text{HAuCl}_4 \cdot 4\text{H}_2\text{O}$ in ethylene glycol (EG) using microwave (MW) heating in the presence of polyvinylpyrrolidone (PVP) as a polymer surfactant. Then, Ni shells were overgrown on Au core seeds by reducing $\text{Ni}(\text{NO}_3)_2 \cdot 6\text{H}_2\text{O}$ in EG with NaOH and PVP using oil bath heating. Resultant crystal structures were characterized using transmission electron microscopic (TEM), high-resolution TEM, TEM–energy dispersed X-ray spectroscopic (EDS), selected area electron diffraction (SAED), and X-ray diffraction (XRD) measurements. Because a very large mismatch (13.6%) exists in lattice constants between Au (0.4079 nm) and Ni (0.3524 nm), the epitaxial growth of Ni shells over Au cores was expected to be difficult. Nevertheless, about 40 monolayers of Ni{111} shells were grown epitaxially on flat planes and sharp corners of Au{111} cores after heating reagent solution at 175 °C for 2 h. The SAED patterns showed Ni layers parallel to Au layers. This result is contrasted with our recent result for Au@Cu with a smaller lattice mismatch between Au and Cu (11.4%). In the case of Au@Cu, although the epitaxial growth of Cu{111} shells over Au core was observed, the growth rate on sharp corners was slower than that on flat {111} facets. Our results and reported data show that the lattice mismatch is not a significant factor for the crystal growth of Au@Ni on sharp corners.



■ INTRODUCTION

Recently, the synthesis of bimetallic nanocrystals consisting of noble metals such as Au, Ag, Pt, and Pd has advanced remarkably, making it possible to generate a wide variety of bimetallic nanostructures with controllable shapes, sizes, and compositions. Typical bimetallic nanocrystals are core–shell structures prepared via heterogeneous, epitaxial growth of polyhedral shells over polyhedral core seeds.^{1–9} In general, there are strong correlations between shapes of cores and shells, so that shape selective preparation of desired morphologies of core–shell particles is possible. For example, we have recently demonstrated that favorable facets of Ag shells over Au{111} cores in Au@Ag core–shell nanocrystals can be changed from {100} in ethylene glycol (EG) to {111} in *N,N*-dimethylformamide (DMF).¹ Therefore, cubic, triangular-bipyramidal, and rod/wire Ag shells with {100} type dominant facets were formed epitaxially over octahedral, triangular platelike, and decahedral Au core seeds with {111} type facets in EG, respectively, whereas the same shapes as those of Au cores with {111} type facets were overgrown on Au core seeds in DMF.

For the rational design and synthesis of bimetallic core–shell nanocrystals with desired shapes, compositions, and thus properties, understanding the heterogeneous nucleation and growth mechanisms is required but still at a rudimentary stage. In a seed-mediated synthesis of bimetallic core–shell nanocrystals, the mode

of heterogeneous nucleation and growth has generally been believed to be mainly determined by physical parameters such as lattice mismatch between core and deposited shell metals. The roles of other parameters such as surface capping, type of facets exposed on the core nanocrystal, bond energies between shell metals and between core and shell metals, electronegativity of core and shell metals, and the reduction kinetics remain largely unexplored.

Recently, Fan et al.⁵ investigated syntheses of bimetallic core–shell nanocubes in aqueous solution using a two-step seed-mediated growth method with octahedral Au cores. Their systematic investigation of the growth of core–shell heterogeneous structures of four typical noble metals (i.e., Au, Ag, Pd, and Pt) revealed the relevant growth modes and general criteria for the conformal epitaxial growth or the heterogeneous nucleation and growth of various noble metals. They found that two different forms exist for the growth of heterogeneous metal shells on the gold core: the conformal epitaxial growth for Au@Pd and Au@Ag nanocubes and the heterogeneous nucleation and island growth for Au@Pt nanospheres. On the basis of results of their systematic studies, they reported that the lattice constants of two metals are expected to be comparable, with

Received: February 11, 2011

Revised: March 20, 2011

Published: March 25, 2011

lattice mismatch of less than about 5%. The validity of this rule has also been confirmed by other researchers for Au@Ag (lattice mismatch, 0.2%), Au@Pd (4.7%), and Pt@Pd (0.85%).^{1–4,6–9}

As compared with extensive studies on core–shell nanocrystals of novel metals such as Au, Ag, Pt, and Pd, little work has been carried out on the shape selective preparation of core–shell nanocrystals involving a transition metal. One reason is that lattice mismatches between novel metals and transition metals with smaller atomic radius are generally much larger than those between two novel metals. The other reason is that the synthesis of transition metals is more difficult than that of novel metals because transition metals are easily oxidized in the presence of oxygen. We have recently investigated the epitaxial growth of Au@Cu nanocrystals using a two-step method to examine effects of lattice mismatch.¹⁰ In our experiment, Cu shells over Au cores were synthesized under bubbling Ar gas to remove oxygen dissolved in a reagent solution. On the basis of transmission electron microscopic (TEM), high resolution (HR)-TEM, TEM–energy dispersed X-ray spectroscopic (EDS), and selected area electron diffraction (SAED) data, we found for the first time that Cu shells can be formed epitaxially on Au cores despite a large lattice mismatch between Au and Cu (11.4%). Our results using various shapes of Au cores also demonstrated that the epitaxial growth rate of Cu layers depends strongly on the positions of cores, for example, flat planes or sharp corners, and epitaxial growth on sharp corners is generally slower than that on flat planes.

The observation of epitaxial growth of Au@Cu nanocrystals led us to conclude that lattice mismatch below 5% is not the definitive factor for the epitaxial growth of metallic nanocrystals and that similar epitaxial growth may occur in other bimetallic systems between a novel metal and a transition metal with a large lattice mismatch. Au–Ni bimetallic nanocrystals with a larger lattice mismatch between Au and Ni (13.6%) than that between Au and Cu (11.4%) have been prepared by a few research groups in solutions, and spherical Au@Ni core–shell particles and Au–Ni spindly nanostructures were obtained.^{11,12} However, to the best of our knowledge, the epitaxial growth of Ni shells on polyhedral Au cores has not been observed. In this study, we investigate the preparation and of Au@Ni nanocrystals using a two-step method to examine whether similar epitaxial growth occurs or not despite a larger lattice mismatch than that of Au@Cu. On the basis of TEM, HR-TEM, TEM-EDS, SAED, and X-ray diffraction (XRD) data, crystal structures of products and their growth mechanisms are studied. Our results show that epitaxial growth is possible for Au@Ni nanocrystals through a similar two-step reduction method. The dependence of the epitaxial growth rate of Ni layers on the positions of cores, for example, flat planes or sharp corners, is examined using a mixture of Au nanocrystals with different shapes as the seeds. The results obtained are compared with those for Au@shell (shell = Ag, Pt, Pd, and Cu) nanocrystals reported previously.^{1,3,5,6,8–10} This work not only provides a simple route to the synthesis of polygonal Au@Ni bimetallic core–shell nanocrystals with controllable morphologies but also greatly advances our understanding of the effects of lattice mismatch and other factors in crystal growth of a typical transition metal such as Ni on the Au nanocrystal surface.

■ EXPERIMENTAL SECTION

For use in this study, HAuCl₄·4H₂O (>99.0%), EG (>99.5%), Ni(NO₃)₂·6H₂O (>98.0%), NaOH (>96.0%), and C₂H₅OH (>99.5%)

were purchased from Kishida Chemical Industry Ltd. and PVP (M_w = 40 k and 55 k in terms of monomeric units) was obtained from Wako Pure Chemical Industries Ltd. and Aldrich, respectively. A high purity Ar gas (>99.999%) was obtained from Japan Fine Products. All reagents were used without further purification.

For this study, Au@Ni core–shell nanocrystals were prepared using a two-step reduction method. In our experiments, EG was used as both a reductant and a solvent. As the first step, Au nanocrystal seeds were prepared by MW heating in EG. In the process, a 2.4 mM concentration of HAuCl₄·4H₂O was dissolved in 20 mL of EG solvent. Then, a 1 M concentration of PVP (M_w = 40 k) was added to the solution above. The whole reaction system was heated for 3 min using MW irradiation in a continuous wave mode (μ reactor, 400 W; Shikoku Keisoku Kogyo K.K.). The solution temperature increased to 198 °C after heating for about 1.5 min; it was kept at this temperature for about 1.5 min. After natural cooling to room temperature, the Au seeds were separated from C₂H₅OH solution by centrifuging the colloidal solution two times at 12000 rpm for 30 min. Then, it was redispersed in a 3 mL EG solution to prepare 3.34 mM Au seed solution. In the second step, 14 mL of EG solution containing 286 mM PVP (M_w = 55 k) was bubbled by Ar gas at a flow rate of 150 mL/min for 10 min and preheated at 175 °C. Subsequently, Au seeds in 3 mL of EG solution were added to the solution described above. Then, 10 mM Ni(NO₃)₂·6H₂O and 666.7 mM NaOH in 3 mL of EG solution were injected dropwise to the solution using a syringe pump at an injection rate of 0.3 mL/min. The final concentrations of Au, Ni, NaOH, and PVP were 0.5, 1.5, 100, and 200 mM, respectively. This indicates that the [Ni]/[Au] molar ratio was 3.0. After all reagents were introduced to the solution in 10 min, the solution was further heated in the oil bath for 110 min. Then, the total heating time after injection of Ni(NO₃)₂·6H₂O was 120 min. Effects of reaction temperature and NaOH concentration for the product structures were examined by changing the solution temperature from 175 °C to 190, 150, 110, or 70 °C and changing the NaOH concentration from 100 to 20 or 400 mM.

The Au@Ni particles were obtained from C₂H₅OH solution by centrifuging the colloidal solution at 15000 rpm for 30 min three times for TEM (JEM-2100XS; JEOL) observations. HR-TEM and TEM-EDS data (2100F; JEOL) and XRD data (Rigaku; RINT-TTR III with Cu K α radiation) were also measured. Extinction spectra of the product solutions were measured in the UV–visible (vis)–near-infrared (NIR) region using a spectrometer (UV-3600; Shimadzu Corp.).

■ RESULTS AND DISCUSSION

Preparation of Au@Ni Nanocrystals at 175 °C and Their Crystal Structures. A mixture of Au nanocrystals of various shapes was prepared to examine effects of crystal shapes of Au seeds in the formation of Au@Ni nanocrystals. Figure 1a portrays a typical TEM image of Au nanocrystals prepared under MW heating, where a mixture of octahedral, triangular and hexagonal platelike, decahedral, and icosahedral Au nanocrystals was observed. The crystal structures of these polygonal particles have been determined by TEM images from various angles and SAED patterns in our previous papers.^{1,13} Results indicated that octahedral particles are single-crystal, triangular and hexagonal plate-like particles are single-twin particles, and decahedral and icosahedral particles are multiple-twin particles, as shown in Figure 1a. All of these seed particles have {111} facets as major planes, except for hexagonal platelike particles, where six {111} and {100} facets appear alternatively on side planes.

The Au@Ni particles were prepared by dropwise injection of Ni(NO₃)₂·6H₂O/NaOH/EG solution to an Au seeds/PVP(55 k)/EG solution preheated to 175 °C under bubbling Ar gas.

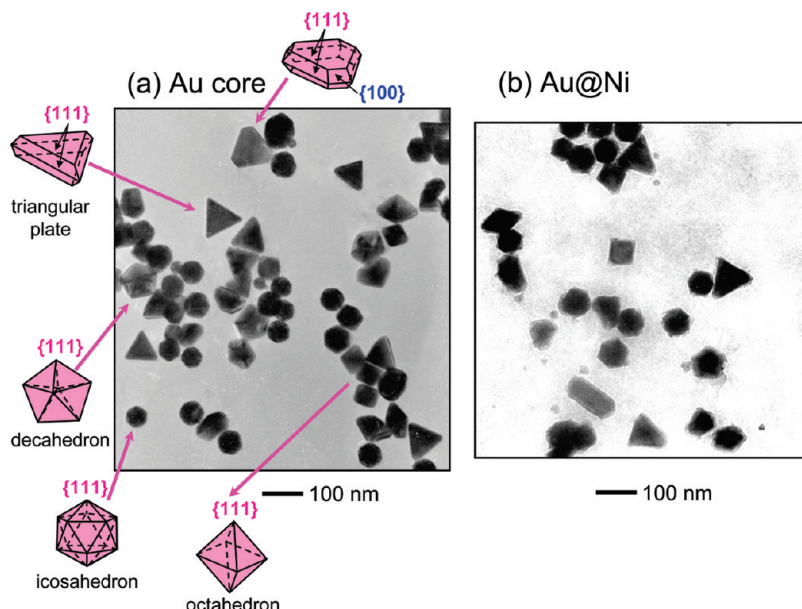


Figure 1. TEM images of (a) Au core and (b) Au@Ni nanocrystals prepared using the polyol method at 175 °C.

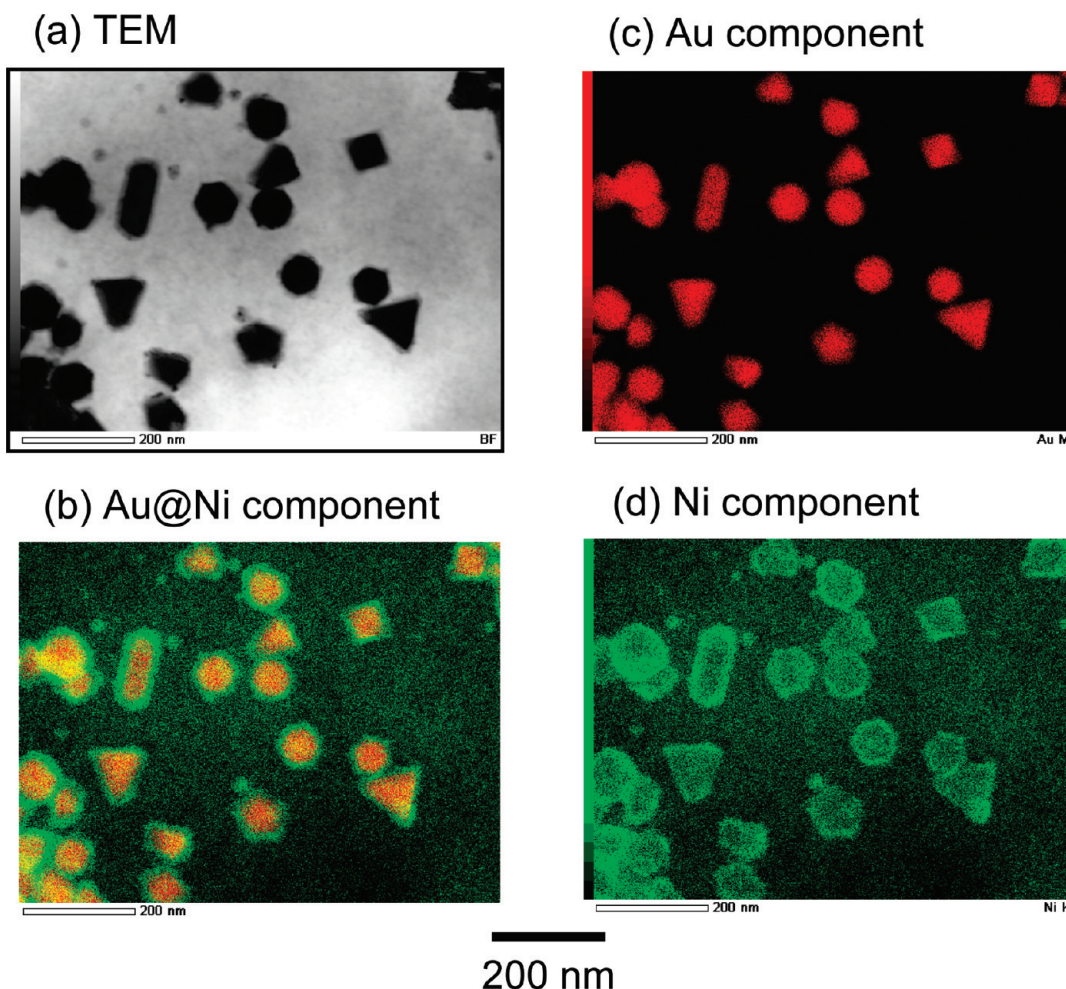


Figure 2. (a) TEM and (b–d) TEM–EDS data of Au@Ni nanocrystals prepared from an Au seeds/ $\text{Ni}(\text{NO}_3)_2 \cdot 6\text{H}_2\text{O}/\text{PVP}(55\text{k})/\text{EG}$ mixture using oil bath heating.

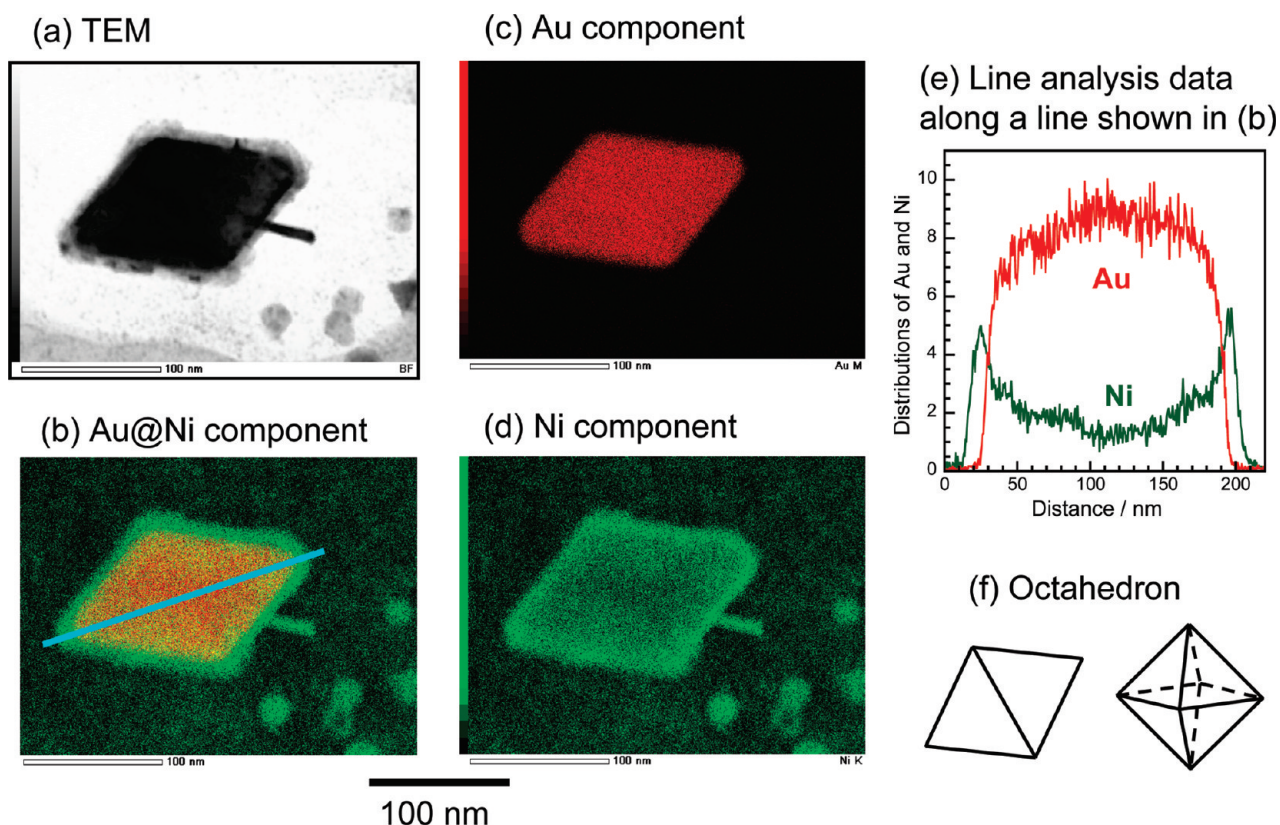


Figure 3. (a) TEM and (b–d) TEM–EDS data of octahedral Au@Ni nanocrystals, (e) line analysis along the line in panel b, and (f) two-dimensional images of octahedral crystal observed from two view angles.

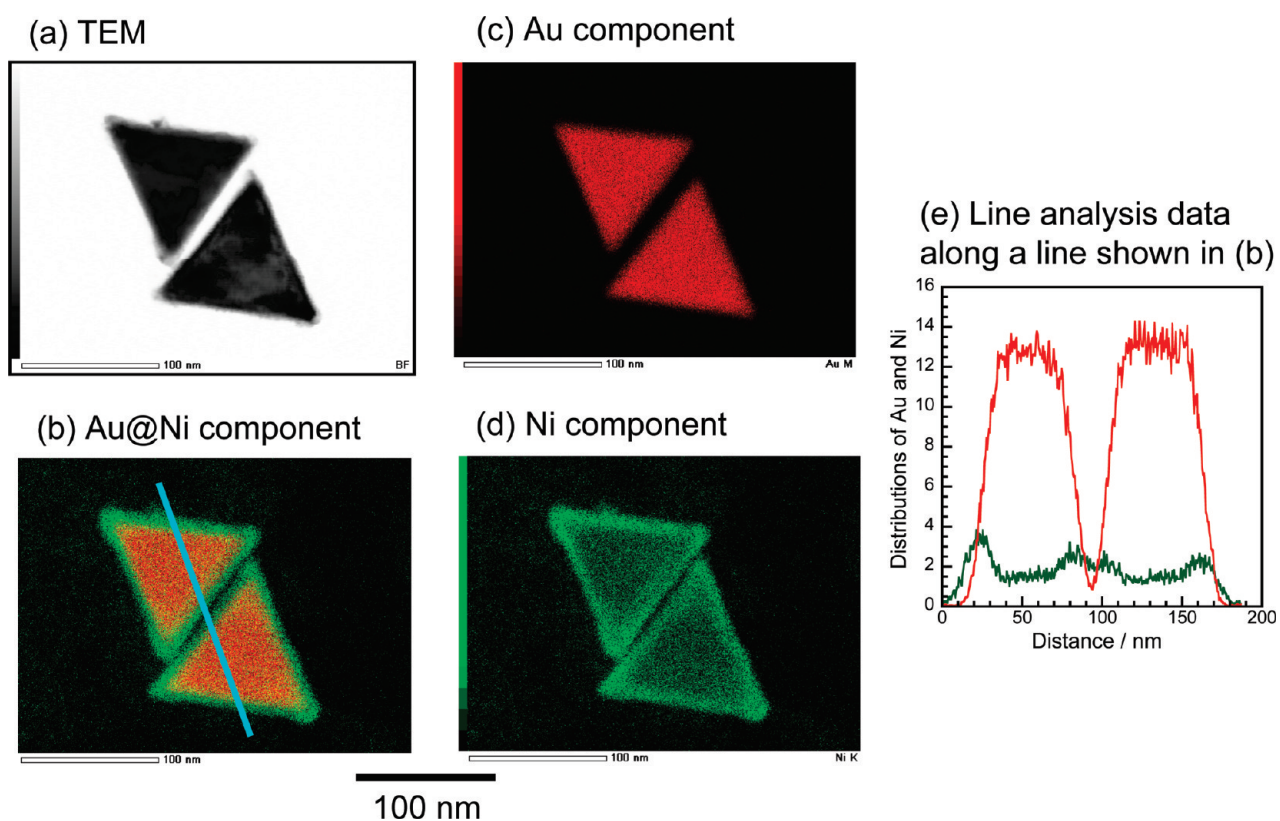


Figure 4. (a) TEM and (b–d) TEM–EDS data of triangular-platelike Au@Ni nanocrystals and (e) line analysis along the line in panel b.

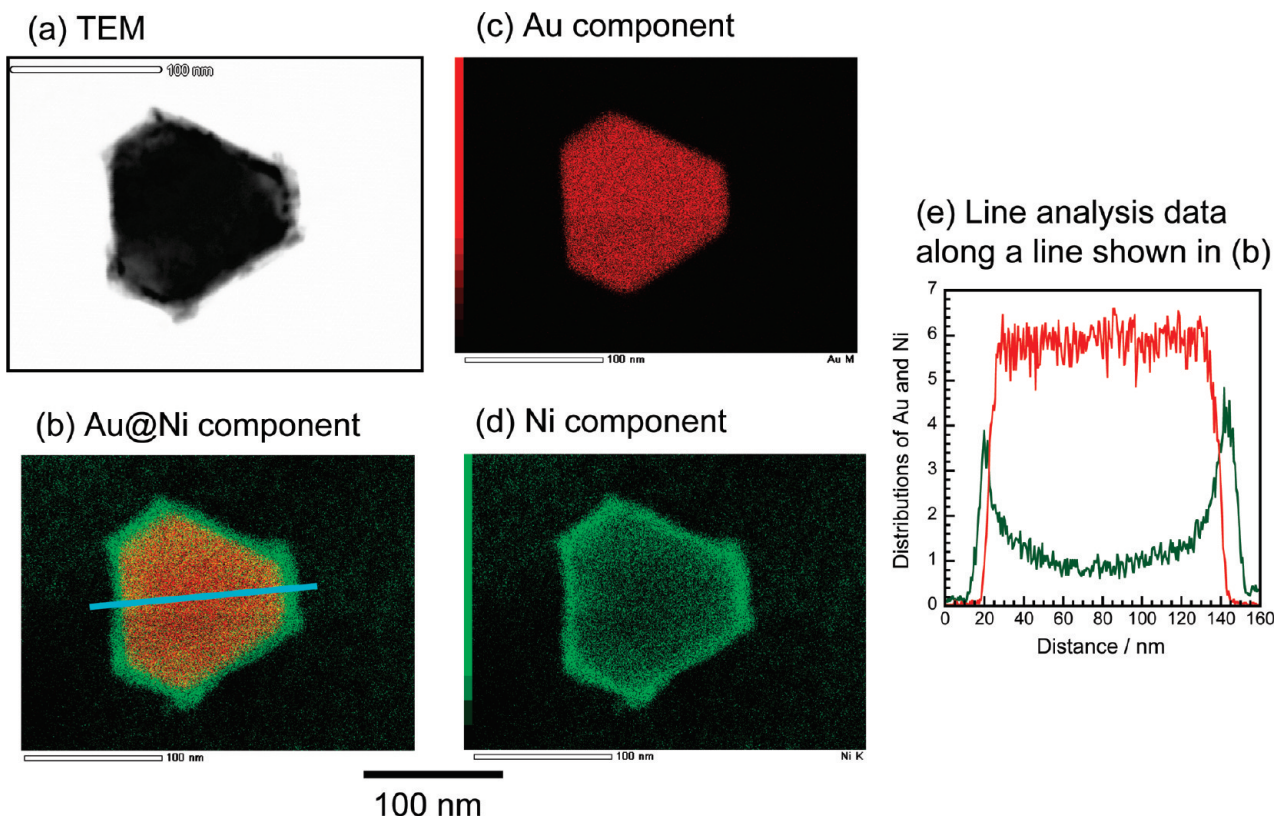


Figure 5. (a) TEM and (b–d) TEM–EDS data of hexagonal platelike Au@Ni nanocrystals and (e) line analysis along the line in panel b.

Although the reduction rate of Cu^{2+} to Cu^0 was much slower than that of Au^{3+} , Cu^{2+} could be reduced to Cu^0 in $\text{Cu}_2(\text{OAc})_4$ /PVP/EG solution at 175 °C in the presence of Au seeds, where EG acts as a main reducing agent.¹⁴ On the other hand, Ni^{2+} cations could not be reduced to Ni^0 without the addition of NaOH as a strong reducing agent, because the standard electrode potential of $\text{Ni}^{2+}/\text{Ni}^0$ (−0.25 eV vs NHE) is lower than that of $\text{Cu}^{2+}/\text{Cu}^0$ (+0.34 eV vs NHE). A typical TEM image of product particles is portrayed in Figure 1b. In most product particles, it seems that dark contrast polygonal Au cores are covered by light contrast Ni shells having the same shapes. However, no definite conclusion can be obtained from only contrast of TEM images whether Ni shells are really grown on Au cores.

To confirm the formation of Au@Ni core–shell structures, TEM-EDS measurements were carried out (Figure 2). The data clarify that Au core components having various shapes are nearly fully covered by Ni shell components. To examine crystals structures and composite distributions in each Au@Ni particle in more detail, expanded TEM-EDS images were measured for octahedral, triangular and hexagonal platelike, decahedral, and icosahedral Au@Ni nanocrystals (Figures 3–6). In each figure, TEM image, EDS data of Au and Ni components, and line analysis data along blue lines in Figures 3b–6b are shown. The TEM-EDS data demonstrate more clearly that each Au core is covered by the same shapes of Ni shells, which implies that the favorable facets of Ni shells are {111} as in the case of Au cores. The distributions of Au component in octahedral, decahedral, and icosahedral Au cores have maxima in the center and decreases greatly on corners or edges (red lines in Figures 3e and 6e), whereas those in triangular and hexagonal platelike particles are rather flat on the plates (red lines in Figures 4e and

Se). The distributions of Ni components have a maximum at the corners or side edges, and they are rather flat on the plane because of uniform coverage of Ni shells (green lines in Figures 3e–6e). On the basis of above EDS analyses of each shape of nanocrystal, Au cores are covered by uniform Ni shells with a thickness of about 10 nm.

SAED patterns were measured by focusing the electron beam perpendicularly on the flat surface of a typical triangular nanoplate (Figure 7a). Part b of Figure 7 portrays a typical SAED pattern measured using a strong electron beam. SAED spots exhibit two sets of hexagonal symmetry patterns in which six heavy white spots corresponding to the {220} reflections of the faced-centered-cubic (fcc) Au and Ni single-crystal orientated in the [111] direction are observed, strongly suggesting that the flat surfaces of the nanoplates are parallel to the {111} plane. Furthermore, a set of weaker spots at the positions of 1/3{422} has been found, indicating a twinning boundary within the Au {111} and Ni {111} planes normal to the TEM electron beam. The 1/3{422} reflections are forbidden for a perfect fcc single-crystalline structure.^{1,13,15,16} In addition to many hexagonal spots, small hexagonal double-diffraction spots of fcc Au and Ni nanocrystals are observed around {220} spots of Au and Ni as shown in Figure 7b, although some of them are partially superimposed with each other.¹⁷ The same SAED patterns attributable to Au and Ni, partially overlapping, are observed on the same lines from the center of diffraction pattern including double-diffraction spots, as in the case of Au@Cu.¹⁰ If NiO is formed as dominant products in Ni shells because of oxidation of Ni, their spots will be observed in similar positions to those of Au because the lattice constant of cubic NaCl type of NiO (0.4177 nm) is similar to that of Au (0.4079 nm) and diffraction spots of Ni

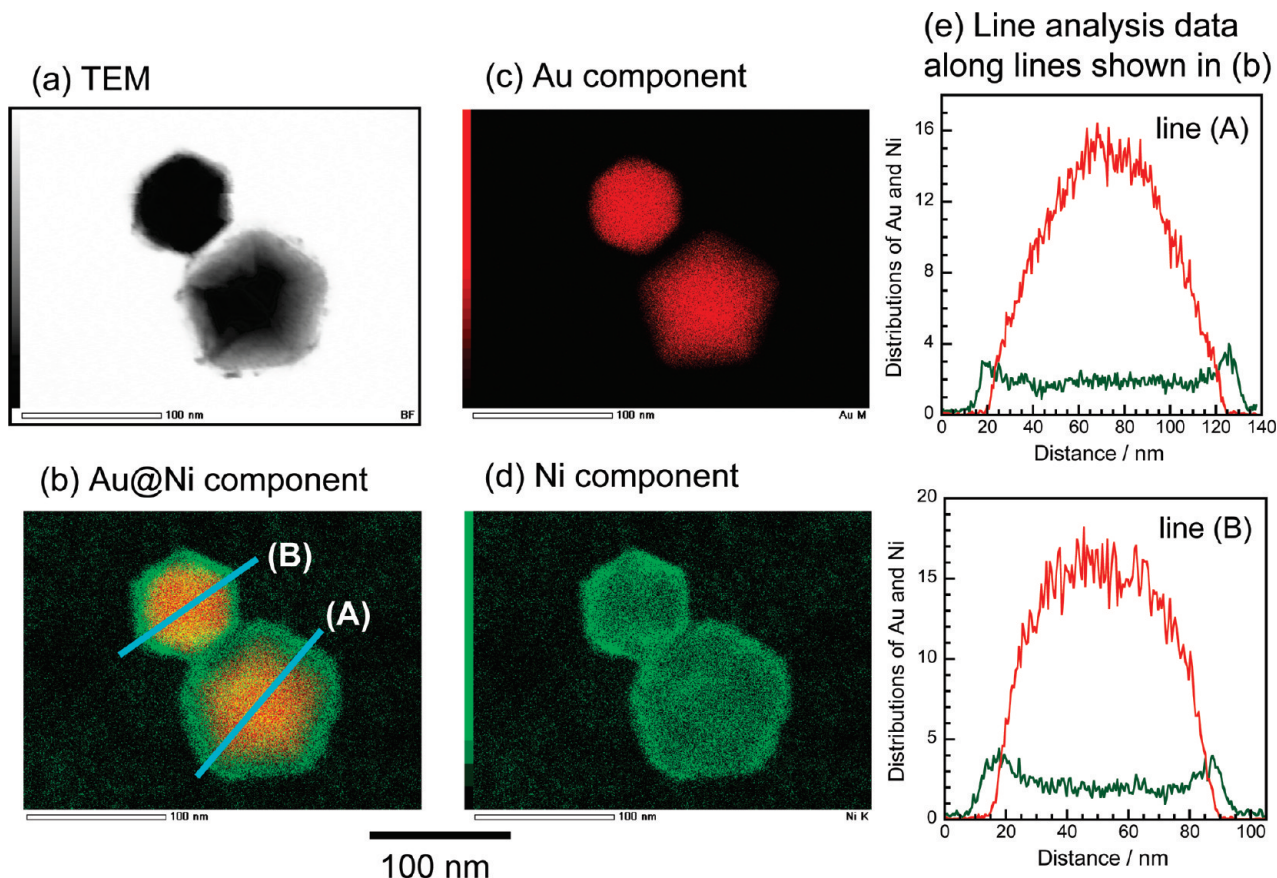


Figure 6. (a) TEM and (b–d) TEM–EDS data of decahedral and icosahedral Au@Ni nanocrystals and (e) line analyses along lines A and B in panel b.

should become weak. The observation of strong spots of Ni and only small fractions of O components in EDS measurements (<atomic content 1%) indicated that contribution of NiO is negligibly small in the product nanocrystals. These results led us to conclude that Ni{111} shell layers of ≈ 10 nm in thickness are grown epitaxially on Au{111} facets despite the presence of a large lattice mismatch between Au (0.4079 nm) and Ni (0.3524 nm), as shown in Figures 3–6. Because the lattice spacing between {110} facets of Ni, which is perpendicular to {111} facets, is 0.249 nm, about 40 monolayers of Ni{111} shells are overgrown on the {111} facets of Au cores. An important finding in this study is that uniform 40 monolayers of Ni shells are epitaxially grown over Au cores, even though the lattice mismatch between Au and Ni (13.6%) is larger than that between Au and Cu (11.4%).

A HR-TEM image was measured for a red circle region of hexagonal nanoplate (Figure 7c), where fringes are observed on the flat facets of Ni shell (Figure 7d). Fringes with a spacing of 0.25 nm were assigned to {110} lattice spacing of the fcc Ni crystal. When the SAED pattern of this hexagonal crystal was observed from the same view angle as that of HR-TEM image, the direction of fringes observed in Figure 7d agreed with the direction of diffraction spots of (220) (Figure 7e). This finding supports that fringes observed in Figure 7d arise from the {110} lattice spacing of Ni single crystal. On the basis of the above facts, we found that the same shapes of Ni shells are epitaxially overgrown on Au cores (Figure 8a-1–a-5). It should be noted that the epitaxial growth rate of Ni shells is essentially independent of shape and position (plain, edge, or corner) of particles for

Au@Ni despite a large lattice mismatch (13.6%). This implies that there is a case that epitaxial growth rate is independent of shape and position of particles in the formation of Au@X nanocrystals (X = transition metal).

Powder XRD patterns of Au core and Au@Ni nanocrystals measured 2 days after synthesis are shown in Figure 9a,b, respectively. The patterns of Au cores indicate the presence of the crystalline gold with fcc structure (2θ equal to 38.2, 44.4, 64.6, 77.6, and 81.7°: PDF 01-073-9564) corresponding to (111), (200), (220), (311), and (222) planes. The diffractions of the crystalline nickel are not as distinct as those of gold because of their weak intensities relative to those of Au and the overlapping with strong Au peaks. Two characteristic peaks of fcc-structured nickel (2θ equal to 51.8 and 76.4°: PDF 01-071-3740) corresponding to (200) and (220) planes can be observed. The (111) peak (2θ equals to 44.5°) is heavily overlapped with the (100) peak of Au (44.4°). Possible oxides or hydroxides such as NiO, Ni₂O₃, or Ni(OH)₂ were not observed. The XRD data indicated that no nickel oxides formed, being consistent with the SAED data.

Effects of Reaction Temperature and NaOH Concentration. To study effects of reaction temperature, we attempted to synthesize Au@Ni nanocrystals at a reaction temperature of 190, 150, 110, or 70 °C. With increasing reaction temperature, the reduction rate of Ni²⁺ to Ni⁰ was expected to increase. Parts a and b of Figure 10 show TEM images of Au@Ni particles obtained at 190 and 150 °C, respectively. At 190 °C, Au cores are covered by uniform Ni shells with an average size of 15 ± 4 nm, which is thicker than that at 175 °C by about 50%. Although Ni shells reserved their shapes of Au cores as shown by red circles in Figure 10a-2, aggregation

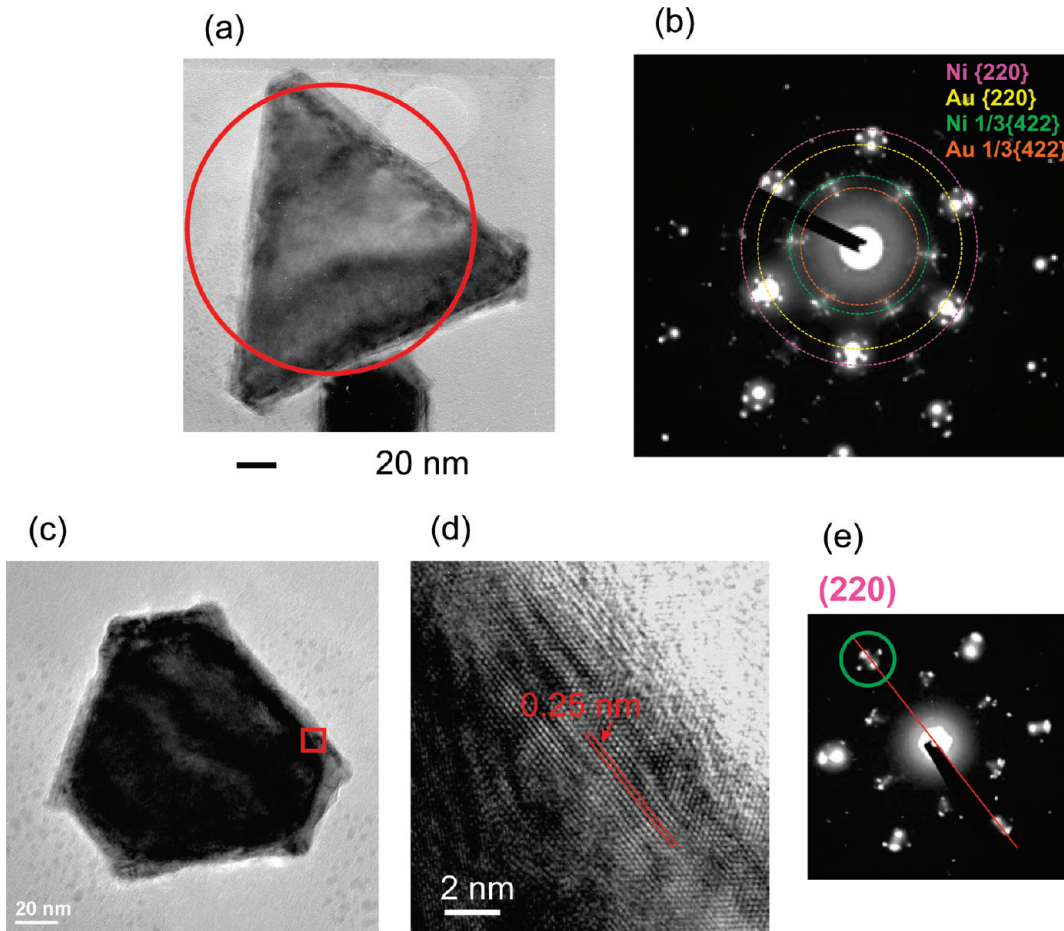


Figure 7. (a) TEM image of triangular-platelike Au@Ni nanocrystal and (b) its SAED pattern. (c) TEM images of hexagonal platelike Au@Ni nanocrystal, (d) HR-TEM image of red part in panel c, and (e) SAED pattern around red part in panel c.

of particles obstructed detailed shape analysis of products. On the basis of TEM images in Figure 10a-2, it seems that the degree of epitaxial growth over Au cores decreased in comparison with slow reduction at 175 °C. At 150 °C, thin Ni shells with an average thickness of 5 ± 1 nm are grown over Au shells. In this case, shapes of Au cores are reserved well in all Ni shells. At 110 and 70 °C, no formation of Au@Ni particles was observed. The above results indicate that the reduction rate is an important factor for the epitaxial growth of Ni shells. In general, slow reduction at low temperatures is favorable for the epitaxial growth of Ni shells, although the thickness of Ni shells decreases with decreasing reaction temperature from 190 to 150 °C.

We succeeded in the preparation of Au@Ni nanoparticles at an NaOH concentration of 100 mM. The effect of NaOH concentration was studied at NaOH concentrations of 20 and 400 mM. At a low NaOH concentration of 20 mM, the reduction rate of Ni^{2+} was too slow to prepare Ni shells, so that no Au@Ni nanocrystal was prepared. On the other hand, at a high NaOH concentration of 400 mM, it was too high, so that Ni^{2+} concentration becomes higher than its supersaturation. Under such a condition, monometallic Ni particles became the dominant product, and little Au@Ni core–shell particles were prepared. These results imply that the controlling reduction rate of Ni^{2+} using an appropriate concentration range of NaOH is also important for the epitaxial growth of Au@Ni nanocrystals.

Growth Mechanisms of Au@Ni Nanocrystals. Fan et al.⁵ pointed out three important factors for the epitaxial layered growth

of heterogeneous core–shell nanocrystals: (i) lattice constants, (ii) electronegativity, and (iii) bond energy. In Table S1 in the Supporting Information are summarized lattice constants, lattice mismatches, atomic radius and bond dissociation energies of Au and Ni metals. For comparison corresponding data for Ag, Pt, Pd, and Cu are also given. Table 1 summarizes relationships of these physical constants for five Au@shell (shell = Ag, Pt, Pd, Cu, and Ni) nanocrystals and the experimental observations for the layered epitaxial growth mode in this study and previous reports.^{1–10} For Au@Ni particles, rule (i) does not hold because of a large lattice mismatch (13.6%). Fan et al.⁵ pointed that the shell metal with smaller atom radius is easier to epitaxially grow on the core as they could uniformly release the lattice strain resulting from the lattice mismatch. Because the atomic radius of Ni (0.124 nm) is smaller than that of Au (0.144 nm), this requirement is satisfied for Au@Ni as in the cases of other four Au@shell (shell = Ag, Pt, Pd, and Cu) nanocrystals. According to rule (ii), the electronegativity of the shell metal should be lower than that of the core metal to avoid the displacement reaction and to wet the surface of the core easily. The standard electrode potential of $\text{Ni}^{2+}/\text{Ni}^0$ (−0.25 eV vs NHE) is lower than that of $\text{Au}^{3+}/\text{Au}^0$ (1.52 eV). The Pauling electronegativity of Ni (1.91) is smaller than that of Au (2.54), which is the highest of any metal. Therefore, rule (ii) holds for Au@Ni particles. On the basis of rule (iii), the bond energy between metal atoms of the shell should be smaller than that between the shell atoms and substrate atoms to ensure growth in the Frank–van der Merwe mode.

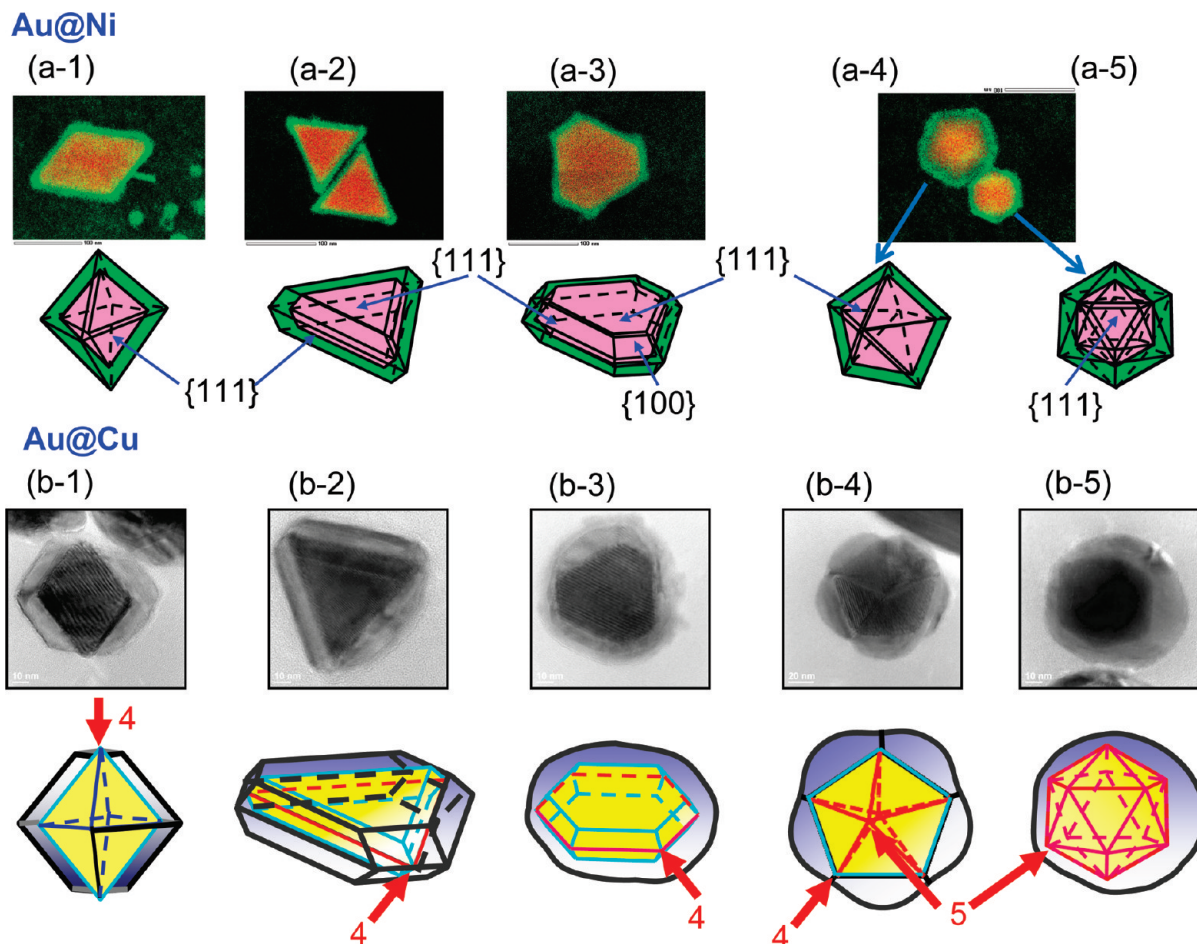


Figure 8. Crystal structures of (a-1)–(a-5) Au@Ni and (b-1)–(b-5) Au@Cu particles (ref 10). Red lines in (b-2)–(b-5) are twin planes in Au cores. Red arrows in (b-2)–(b-5) are corners in which more than four facets mutually intersect. For the sake of clarity, only typical positions are indicated by red arrows; numbers 4 or 5 represent the total numbers of facets located on each corner.

Actually, the bond energy of Ni–Ni ($203.26 \pm 0.96 \text{ kJ mol}^{-1}$) is less than that of Au–Ni ($247 \pm 21 \text{ kJ mol}^{-1}$),^{18,19} showing that this rule also holds for Au@Ni particles. Consequently, two of three rules hold in the present Au core Ni shell system, as in the case of Au@Cu particles (see related data in Table S1 in the Supporting Information). We have recently found that the lattice mismatch in rule (i) can be expanded to 11.4% in Au@Cu particles.¹⁰ This work for Au@Ni shows that the limited value of lattice mismatch for the epitaxial growth can be further expanded from 11.4 to 13.6%. As shown in Table 1, the conformal epitaxial growth does not occur for Au@Pt for which the heterogeneous nucleation and island growth take place. Although bond dissociation energies of Ag–Ag, Pd–Pd, Cu–Cu, and Ni–Ni are smaller than that of Au–Au, the opposite relation holds for Pt–Pt (Table S1 in the Supporting Information). Thus, rule (iii) may be more important than rule (i) for the epitaxial growth of metallic shells over Au cores.

We were able to synthesize Ni nanocrystals having well-defined facets in the presence of Au cores as thin Ni shells at 175 °C. In all cases, the shapes of Au cores are reserved well, leading us to conclude that the mismatch of two metals (13.6%) is not a significant factor for the epitaxial growth of Ni over Au. According to previous studies on the preparation of core–shell nanocrystals, the growth rate of shell layers is independent of shape and position (plain, edge, or corner) of particles for Au@Ag, Au@Pd, and Pd@Pt nanocrystals having small lattice

mismatches below $\leq 4.7\%$,^{1–9} and core particles are covered by uniform shell particles. On the other hand, the growth rate of shell particles strongly depends on the shape and position of core particles for Au@Cu nanocrystals having a large lattice mismatch (11.4%).¹⁰ We found that the epitaxial growth of the Cu shell on sharp corners was much slower than that on flat planes, irrespective of the presence and number of twin planes, as shown in Figure 8b-1–b-5. We have previously discussed the dependence of growth rate on the position in terms of numbers of neighboring facets and defects in product particles.¹⁰ Numbers of facets on the corners are shown in Figure 8b-1–b-5 by red ink. To form Cu epitaxial layers on each polygonal core particle on the sharp corners, four or five neighboring facets must be mutually matched in every layer. Cu shells have some distortion because of a large mismatch in Au@Cu (11.4%). Such a distortion of Cu shell layers suppresses the epitaxial growth rate of the Cu shell, especially on the corners. Decahedral and icosahedral particles, which are composed of 5 and 20 tetrahedral units, respectively, have some defects, especially in edge parts.^{1d,10,20,21} We predicted that the presence of such defects is another reason why epitaxial growth of perfect shapes of Cu shells is difficult on multiple-twin decahedral and icosahedral Au particles.

In this work, we found that the epitaxial growth occurs for Au@Ni nanocrystals, being independent of the shape and position of Au cores, despite a larger lattice mismatch (13.6%)

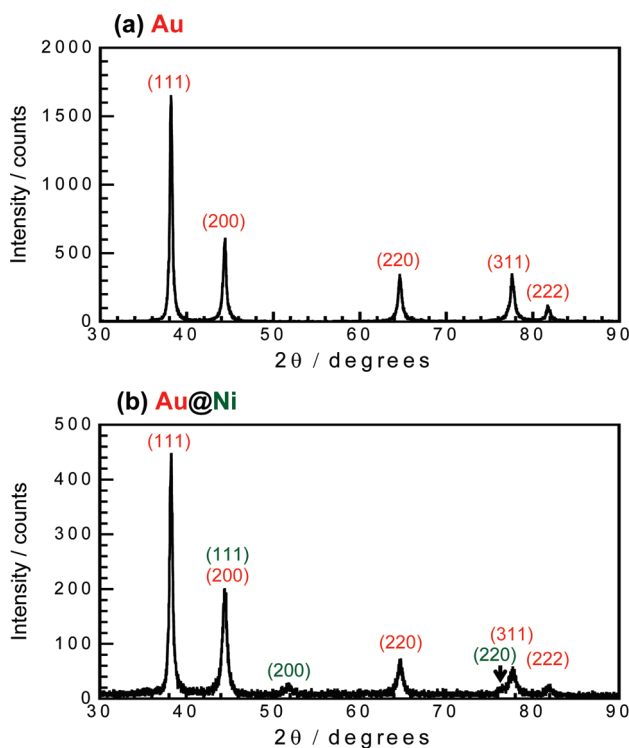


Figure 9. Powder XRD patterns of (a) Au core and (b) Au@Ni core–shell nanocrystals measured 3 days after synthesis. Planes of fcc-structured Au and Ni are shown by red and green colors, respectively.

than that of Au@Cu (11.4%). This implies that the large lattice mismatch does not suppress the epitaxial growth rate even on sharp corners for Au@Ni.

The epitaxial growth of bimetallic systems has been studied using gas-phase deposition (e.g., molecular beam epitaxy)²² and a solution-phase electrochemical method.²³ In the presence of a strong size mismatch between the elements, a large interfacial stress is expected in the pseudomorphic state, which can be relieved by various mechanisms: atomic relaxations,²⁴ formation of misfit dislocations,^{25–28} or interfacial mixing of two metals.²⁹ Labat et al.³⁰ studied stresses and interfacial structure in Au–Ni metallic multilayers. They combined plate bending measurements and electron or XRD to investigate stress buildup and interfacial mixing. Their results show that stress buildup during the growth of Ni on Au(111) is dominated by segregation of Au to the surface. The segregation of Au to the surface results in interfacial mixing of Au and Ni, which decreases the elastic stress. Similar segregation of Au cores to Ni shells may occur during formation of Au@Ni nanocrystals in this study to reduce stress in interfaces. A more detailed investigation of the interface structure is required to verify the mechanisms by which the interface strain is relaxed in Au@Ni and Au@Cu nanocrystals and the layer-by-layer growth can occur on not only flat planes but also sharp corners for Au@Ni despite a larger lattice mismatch. Although what kind of interface is created between two metal layers is essential for the epitaxial growth of shell layers, orientation of Ni atoms in outer shell layers is the same as that of core layers, even insertion of interfaces between cores and shells in the cases of Au@Ni and Au@Cu.

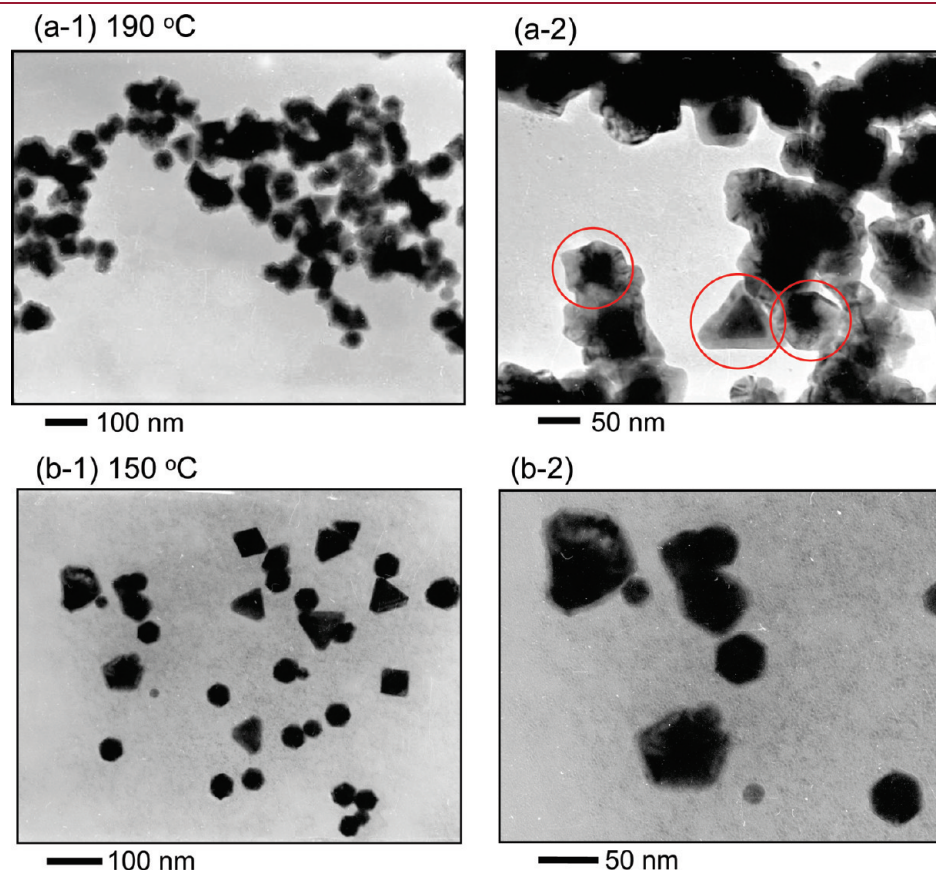


Figure 10. TEM images of Au@Ni nanocrystals prepared using the polyol method at (a) 190 and (b) 150 °C.

Table 1. Comparison of Physical Constants between the Core Metal and the Shell Metal in Au@shell (Shell = Ag, Pt, Pd, Cu, and Ni) Nanocrystals^a

Au@shell	lattice mismatch (%)	atomic radius $r_{\text{core}} \text{ vs } r_{\text{shell}}$	bond dissociation energies $E_{\text{core-core}} \text{ vs } E_{\text{shell-shell}}$	electronegativity (Paulings) $X_{\text{core}} \text{ vs } X_{\text{shell}}$	experimental observation of epitaxial growth ^b
Au@Ag	0.2	equal	high	high	yes
Au@Pt	3.8	large	low	high	no
Au@Pd	4.6	large	high	high	yes
Au@Cu	11.4	large	high	high	yes
Au@Ni	13.6	large	high	high	yes

^a The related physical constants of various kinds of noble metal are listed in Table S1 in the Supporting Information. ^b Refs 1–10.

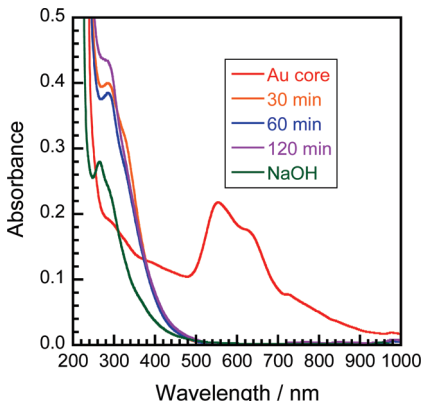


Figure 11. (a) Time dependence of UV–vis–NIR spectra of Au@Ni nanocrystals prepared from Au seeds/Ni(NO₃)₂·6H₂O/PVP(55 k)/EG solution at 175 °C.

Besides lattice mismatch and other factors shown above, various kinetic factors probably govern the epitaxial growth of Au@Ni. For example, we have shown that the controlling the reduction rate of Ni²⁺ by changing solution temperature or NaOH concentration is important for the epitaxial growth of Au@Ni. These results imply that kinetic parameters in the synthesis also play significant roles for the epitaxial growth of core–shell particles. In general, slow reduction of metallic cations keeping the concentration of metal atoms below supersaturation is required for the epitaxial growth of core–shell particles having large lattice mismatches.

UV–vis–NIR Spectra of Au@Ni Particles. The UV–vis–NIR spectra were measured to characterize optical properties and to elucidate the time evolution of Au@Ni particles (Figures 11). The SPR band of Au core particles with a peak at ≈550 nm is observed in the 250–1000 nm region. After heating for 30 min, the SPR band of Au core disappears, and a long tail band is observed in the 250–550 nm region with a peak at 290 nm. The spectra at 60 and 120 min were similar to that at 30 min, indicating that the reduction of Ni was completed at 30 min. It is known that SPR band of Ni gives a long tail band with a strong peak at 210 nm and a weak shoulder peak at 350 nm.³¹ The appearance of strong peak at 210 nm in Figure 11 agrees well with that of Ni particles, showing that Au@Ni particles have optical properties of Ni shells. The optical properties of Au@Ni reflect those of shell metal are consistent with our previous results of Au@Cu¹⁰ and Ag@Ni³² for which intensities of SPR bands of Au and Ni shells are much weaker than those of Au and Ag core particles.

CONCLUSION

We have recently found that the epitaxial layered growth of Cu shells over polygonal Au cores rarely occurs despite a lattice mismatch of Au and Cu as great as 11.4%.¹⁰ In this study, we demonstrated that the epitaxial layered growth of Ni shells over polygonal Au cores can also occur despite a larger lattice mismatch of Au and Ni (13.6%). Favorable facets of Ni shell were {111}, which were the same as the major facets of Au core seeds, as in the case of Au@Cu.¹⁰ The SAED patterns indicated that single crystals of Ni layers formed parallel to those of Au seeds. For Au@Ni crystals, Ni shells were grown not only on flat {111} planes but also sharp corners of Au cores with the same thickness. This result was different from the case of Au@Cu, where the growth rates of Cu shells on sharp corners of Au cores were slower than those on flat {111} facets and single-twin facets. Our present results indicated there is an exceptional case that epitaxial growth can occur on sharp corners even though the lattice mismatch is as large as 13.6%. A HR-TEM observation and XRD measurements near boundary layers are necessary to clarify the mechanism of epitaxial growth of Ni shells over flat planes and sharp corners of Au{111} cores. The UV–vis–NIR spectra of Au@Ni nanoparticles gave a similar spectrum to that of Ni particle, indicating that Au@Ni particles have similar optical properties to those of Ni shells.

ASSOCIATED CONTENT

S Supporting Information. Physical constants of noble and transition metals. This material is available free of charge via the Internet at <http://pubs.acs.org>.

AUTHOR INFORMATION

Corresponding Author

*E-mail: tsuji@cm.kyushu-u.ac.jp.

ACKNOWLEDGMENT

This work was supported by a Grant-in-Aid for Scientific Research (B) from the Ministry of Education, Culture, Sports, Science, and Technology of Japan (MEXT, No. 22310060) and by the Management Expenses Grants for National Universities Corporations from the MEXT.

REFERENCES

- (a) Tsuji, M.; Miyamae, N.; Lim, S.; Kimura, K.; Zhang, X.; Hikino, S.; Nishio, M. *Cryst. Growth Des.* **2006**, *6*, 1801. (b) Tsuji, M.; Matsuo, R.; Jiang, P.; Miyamae, N.; Ueyama, D.; Nishio, N.; Hikino, S.; Kumagae, H.; Kamarudin, K. S. N.; Tang, X.-L. *Cryst. Growth Des.* **2008**,

- 8, 2528. (c) Tsuji, M.; Nishio, M.; Jiang, P.; Miyamae, N.; Lim, S.; Matsumoto, K.; Ueyama, D.; Tang, X. *Colloids Surf., A* **2008**, *317*, 247.
- (d) Tsuji, M.; Ogino, M.; Matsunaga, M.; Miyamae, N.; Matsuo, R.; Nishio, M.; Alam, M. *J. Cryst. Growth Des.* **2010**, *10*, 4085.
- (2) Xiang, Y.; Wu, X.; Liu, D.; Jiang, X.; Chu, W.; Li, X.; Ma, Y.; Zhou, W.; Xie, S. *Nano Lett.* **2006**, *6*, 2290.
- (3) Xue, C.; Millstone, J. E.; Li, S.; Mirkin, C. A. *Angew. Chem., Int. Ed.* **2007**, *46*, 8436.
- (4) Habas, S. E.; Lee, H.; Radmilovic, V.; Somorjai, G. A.; P. Yang, P. *Nat. Mater.* **2007**, *6*, 692.
- (5) Fan, F.-R.; Liu, D.-Y.; Wu, Y.-F.; Duan, S.; Xie, Z.-X.; Jiang, Z.-Y.; Tain, Z.-Q. *J. Am. Chem. Soc.* **2008**, *130*, 6949.
- (6) Wu, Y.; Jiang, P.; Jiang, M.; Wang, T.-W.; Guo, C.-F.; Xie, S.-S.; Wang, Z.-L. *Nanotechnology* **2009**, *20*, 305602.
- (7) Lee, Y. W.; Kim, M.; Kim, Z. H.; Han, S. W. *J. Am. Chem. Soc.* **2009**, *131*, 17036.
- (8) (a) Lim, B.; Wang, J.; Camargo, P. H. C.; Jiang, M.; Kim, M. J.; Xia, Y. *Nano Lett.* **2008**, *8*, 2535. (b) Lim, B.; Kobayashi, H.; Yu, T.; Wang, J.; Kim, M. J.; Li, Z.-Y.; Rycenga, M.; Xia, Y. *J. Am. Chem. Soc.* **2010**, *132*, 2506. (c) Jiang, M.-J.; Lim, B.; Tao, J.; Camargo, P. H. C.; Ma, C.; Zhu, Y.-M.; Xia, Y.-N. *Nanoscale* **2010**, *2*, 2406. (d) Ma, Y.-Y.; Li, W.-Y.; Cho, E.-C.; Li, Z.-Y.; Yu, T.-K.; Zeng, J.; Xie, Z.-X.; Xia, Y.-N. *ACS Nano* **2010**, *4*, 6725.
- (9) Tsuji, M. Core Shell Particles. In *Shape and Structure Control of Metal Nano- and Fine-Particles*; Yonezawa, T., Eds.; CMC: Tokyo, 2009; p 166 (in Japanese).
- (10) Tsuji, M.; Yamaguchi, D.; Matsunaga, M.; Alam, M. *J. Cryst. Growth Des.* **2010**, *10*, 5129.
- (11) Zhang, H. T.; Ding, J.; Chow, G. M.; Ran, M.; Yi, J. B. *Chem. Mater.* **2009**, *21*, 5222.
- (12) Wang, D.-S.; Li, Y.-D. *J. Am. Chem. Soc.* **2010**, *132*, 6280.
- (13) (a) Tsuji, M.; Hashimoto; Nishizawa, Y.; Tsuji, T. *Chem. Lett.* **2003**, *32*, 1114. (b) Tsuji, M.; Hashimoto, M.; Nishizawa, Y.; Kubokawa, M.; Tsuji, T. *Chem.—Eur. J.* **2005**, *11*, 440. (c) Tsuji, M.; Miyamae, N.; Hashimoto, M.; Nishio, M.; Hikino, S.; Ishigami, N.; Tanaka, I. *Colloids Surf., A* **2007**, *302*, 587. (d) Tsuji, M.; Miyamae, N.; Nishio, M.; Hikino, S.; Ishigami, N. *Bull. Chem. Soc. Jpn.* **2007**, *80*, 2024.
- (14) (a) Tsuji, M.; Hikino, S.; Sano, Y.; Horigome, M. *Chem. Lett.* **2009**, *38*, 518. (b) Tsuji, M.; Hikino, S.; Tanabe, R.; Sano, Y. *Chem. Lett.* **2009**, *38*, 860. (c) Tsuji, M.; Hikino, S.; Tanabe, R.; Yamaguchi, D. *Chem. Lett.* **2010**, *39*, 334. (d) Tsuji, M.; Hikino, S.; Tanabe, R.; Matsunaga, M.; Sano, Y. *CrystEngComm* **2011**, *12*, 3900.
- (15) Kirkland, A. I.; Jefferson, D. A.; Duff, D. G.; Edwards, P. P.; Gameson, I.; Johnson, B. F. G.; Smith, D. J. *Proc. R. Soc. London A* **1993**, *440*, 589.
- (16) Germain, V.; Li, J.; Ingert, D.; Wang, Z. L.; Pilani, M. P. *J. Phys. Chem. B* **2003**, *107*, 8717.
- (17) Williams, D. B.; Carter, C. B. *Transmission Electron Microscopy, A Textbook for Materials Science*, 2nd ed.; Springer: New York, 2009.
- (18) Lide, D. R., Ed. *CRC Handbook of Chemistry and Physics*, 81st ed.; CRC Press: Boca Raton, FL, 2000.
- (19) Kant, A. *J. Chem. Phys.* **1968**, *49*, 5144.
- (20) Xia, Y.; Xiong, Y.; Lim, B.; Sara, E.; Skrabalak, S. E. *Angew. Chem., Int. Ed.* **2009**, *48*, 60.
- (21) Tsuji, M.; Ogino, M.; Matsuo, R.; Kumagae, H.; Hikino, S.; Kim, T.-G.; Yoon, S.-H. *Cryst. Growth Des.* **2010**, *10*, 296.
- (22) Jaeger, R. C. *Film Deposition. Introduction to Microelectronic Fabrication*; Prentice Hall: Upper Saddle River, 2002.
- (23) Hwang, S.; Oh, I.; Kwak, J. *J. Am. Chem. Soc.* **2001**, *123*, 7176.
- (24) Mottet, C.; Tréglia, G.; Legrand, B. *Phys. Rev. B* **1992**, *46*, 16018.
- (25) Jacobsen, J.; Nielsen, L. P.; Besenbacher, F.; Stensgaard, I.; Lægsgaard, E.; Rasmussen, T.; Jacobsen, K. W.; Norskov, J. K. *Phys. Rev. Lett.* **1995**, *75*, 489.
- (26) Günther, C.; Vrijmoeth, J.; Hwang, R. Q.; Behm, R. *J. Phys. Rev. Lett.* **1995**, *74*, 754.
- (27) Hamilton, J. C.; Foiles, S. M. *Phys. Rev. Lett.* **1995**, *75*, 882.
- (28) Brune, H.; Röder, H.; Boragno, C.; Kern, K. *Phys. Rev. B* **1994**, *49*, 2997.
- (29) Meunier, I.; Tréglia, G.; Gay, J.-M.; Aufray, B.; Legrand, B. *Phys. Rev. B* **1999**, *59*, 10910.
- (30) Labat, S.; Bocquet, F.; Gilles, B.; Thomas, O. *Scr. Mater.* **2004**, *50*, 717.
- (31) (a) Tsuji, M.; Hashimoto, M.; Tsuji, T. *Chem. Lett.* **2002**, *31*, 1232. (b) Creighton, J. A.; Eadon, D. G. *J. Chem. Soc. Faraday Trans. 1991*, *87*, 3881.
- (32) Tsuji, M.; Hikino, S.; Matsunaga, M.; Sano, Y.; Hashizume, T.; Kawazumi, H. *Mater. Lett.* **2010**, *1793*.